*J. Mater. Environ. Sci. 4 (6) (2013) 953-960*
*ISSN : 2028-2508*
*CODEN: JMESCN*



# Influence of tungsten on the anatase-rutile phase transition of sol-gel synthesized $TiO_2$ and on its activity in the photocatalytic degradation of pesticides

**M. Abdennouri[1], R. Elmoubarki[1], A. Elmhammedi[1], A. Galadi[2], M. Baâlala[3], M. Bensitel[3], A. Boussaoud[4], Y. El hafiane[5], A. Smith[6], N. Barka[1,*]**

[1] *Université Hassan 1, Laboratoire CAE, Equipe de Recherche Gestion de l'Eau et Développement Durable (GEDD), Faculté Polydisciplinaire de Khouribga, BP. 145 Khouribga, Morocco.*
[2] *ERACE, Ecole Supérieure de Technologie de Safi, Université Cadi Ayyad, BP. 89, Route Dar Si Aissa, Safi, Morocco.*
[3] *LCCM, Faculté des Sciences, Université Chouaib Doukkali, Route Ben Maachou BP. 20, 24000, El Jadida, Morocco.*
*4 Faculté Polydisciplinaire de Safi, B.P: 416, Route Sidi Bouzid, 46000, Safi, Morocco.*
[5] *LMPEQ, Ecole Nationale des Sciences Appliquées de Safi, Université Cadi Ayyad, Sidi Bouzid, BP.63 Safi 46000, Morocco.*
[6] *GEMH, Ecole Nationale Supérieure de Céramique Industrielle, Centre Européen de la Céramique, 12 rue Atlantis, 87068 Limoges cedex, France.*

Received 15 April 2013, Revised 8 June 2013, Accepted 8 June 2013
** Corresponding author:* Email : barkanoureddine@yahoo.fr; *Tel.: +212 661 66 66 22; fax: +212 523 49 03 54*

## Abstract
In the present study, titanium dioxide and tungsten-modified titanium dioxide photocatalysts were synthesized by sol–gel method. Structural and morphological characterization has been carried out by using X-ray powder diffraction (XRD), FT-IR spectroscopy, BET surface area and transmission electron microscopy (TEM) coupled to the energy dispersive spectroscopy (EDX). The adsorption and photocatalytic performances were investigated using two chlorophenoxy herbicides; 2,4-dichlorophenoxyacetic acid (2,4-D) and 2-(2,4-dichlorophenoxy) propionic acid (2,4-DP) as models of organic pollutants in water. The obtained results show that addition of tungsten to the sol-gel preparation of $TiO_2$ delayed the conversion of anatase to rutile phase. Further increase in tungsten loading apparently stabilized the anatase phase from transformation into inactive rutile. It is also found that, tungsten doped $TiO_2$ exhibited a remarkable enhancement of the photocatalytic activity compared with the unmodified $TiO_2$ for the photodegradation of the two selected organochlorines herbicides.

*Keywords*: Tungsten-modified titania, Photocatalysis, Pesticides, Anatase, Rutile.

## 1. Introduction
Oxidative degradation of organic pollutants in aqueous phase using a photo-illuminated catalyst surface has emerged as a potential technology for treating wastewater effluents [1,2]. This emerging technique offers a unique advantage over other alternative treatment methods because it presents a 'green' treatment approach; since, toxic organic pollutants are converted into carbon dioxide ($CO_2$) and water using photonic energy [1–7].
Heterogeneous photocatalysis is based upon the use of UV-irradiated semiconductors. When the semiconductor is irradiated with photons whose energy is equal to or greater than its band gap energy, electron-hole pairs are created. In aqueous system, holes react with $H_2O$ or $OH^-$ adsorbed at the surface of the semiconductor to produce OH° radicals which are the most oxidizing species in this process [8].
As a chemically stable, highly efficient, non-toxic, and relatively inexpensive photocatalyst, titanium dioxide ($TiO_2$) has received the most attention in water and air purification since many environmental pollutants can be degraded by decomposition and oxidation processes on its surface. However, $TiO_2$ catalysts cannot absorb visible light and only make use of 3–5% of the solar spectrum due to a large band gap.
Several methods were adopted for the synthesis of the titanium dioxide. The most conventional one is the sol-gel method which depends entirely on precursors of departure [10-12]. At present, diverse efforts have been

made toward modifying titanium dioxide and testing other semiconductors to identify ways to increase process efficiency and to improve the overlap of the absorption spectrum of the photocatalyst with the solar spectrum.
The titanium dioxide exists under several crystalline forms among which three main clauses are the anatase, the brookite and the rutile. By rise of temperature, the anatase phase is transformed in brookite then in rutile phase. Rutile is the thermodynamically stable state, whereas the other two phases are metastable [9]. Commercially we find it in the shape of anatase, rutile or a mixture of these two structures.
Modification with certain metals such as Ni [13], Fe [13,14], Th [14], Cu [14], V and Mo [15], Co [16], Sn [17], and Ag [18], may alter the phase transformation of $TiO_2$ from active anatase to inactive rutile by lowering the activation energy. The activation energy is further affected by metal dosage and method of preparation. On the other hand, metals such as Mg and Ba [19], Mn [20], Tb, Eu and Sm [21], La [22], and Sc and Nb [23] have been reported to inhibit transformation phase.
Among transition metal dopants, cobalt and tungsten are reportedly the best for the photodegradation of 4-nitrophenol, benzoic acid, and methanoic acid [24–26].The addition of tungsten to $TiO_2$ has been observed to improve activity under visible-light irradiation for the degradation of dodecyl-benzenesulfonate [27], methyl orange [28] and 2,4-dihydroxyanisole [29] and methylene blue [30].
The objective of this study was to evaluate the effect of $TiO_2$ modification with tungsten, using impregnation method, on the photocatalytic degradation of 2,4-dichlorophenoxyacetic acid and 2-(2,4-dichlorophenoxy) propionic acid. Characterization of the photocatalysts was carried out using X-ray powder diffraction (XRD), FT-IR spectroscopy, BET surface area and transmission electron microscopy (TEM) coupled to the energy dispersive spectroscopy (EDX).

## 2. Materials and methods

*2.1. Materials*

All reagents used in this work were of analytical grade and were used without any further purification; titanium tetraisopropoxide ($Ti(OC_3H_7)_4$, Fluka company, 98% purity), tungsten hexacarbonyl ($C_6O_6W$, Sigma-Aldrich Chemical Company, 97% purity), absolute ethanol ($C_2H_6O$, Prolalo, 99.85%), methanol (Prolalo, 97%), diethyl ether ($C_4H_{10}O_3$, Loba Chimie society), 2,4-dichlorophenoxyacetic acid ($C_8H_6Cl_2O_3$, Fluka company, 95% purity) and 2,4-dichlorophenoxypropionic acid ($C_9H_8Cl_2O_3$, Sigma-Aldrich Chemical Company, 95% purity). The solutions were prepared with pure distilled water obtained from a Millipore Milli-Q laboratory system.

*2.2. Preparation and characterization of x%-W/$TiO_2$ photocatalysts*

At first, the nanosized titanium dioxide powder was prepared by dissolving titanium tetraisopropoxide (Ti(OC3H7)4 in methanol/ethanol solution with molar ratio of 1:1:10 [12]. The obtained solution was maintained at 75°C for three hours and an appropriate amount of distilled water was added drop wise into the aforesaid solution. After gelling, the sample was separated by filtration. The obtained solid was dried at 110°C during a night then calcined at 500°C for 4 hours.
The 0.5%-W/$TiO_2$**,** 1%-W/$TiO_2$, 1.5%-W/$TiO_2$, 2%-W/$TiO_2$ and 4%-W/$TiO_2$ samples were prepared by standard wet impregnation method of a dried $TiO_2$ powder. The impregnation was carried out by dissolving the appropriate amounts of tungsten hexacarbonyl ($C_6O_6W$) in diethyl ether. This solution was then added to the dried $TiO_2$. The impregnated products were then dried and calcined as described above to achieve total decomposition of $C_6O_6W$ to $WO_3$.
The phases present in the photocatalysts and their crystallinity were determined by powder X-ray diffraction method. The pattern was registered from 2θ of 20 to 80° at scan rate of 2°/min. An X'Pert Hight Score diffractometer was used. The radiation was Kα of Cu. The accelerating voltage and the applied current were 40 kV and 35 mA, respectively.
The ratios of rutile/anatase were determined by XRD according to the method described by Jung et al. [32] as follows:

$$\%\,\text{Rutile} = \frac{1}{((\frac{A}{R}) \times 0.884 + 1))} \times 100 \qquad \text{(Eq.1)}$$

where, A and R are the peak area for major anatase (2θ=25.3°) and rutile phase (2θ= 31.6°), respectively.

The crystallines sizes of the prepared samples were determined from X-ray line broadening determined as follows:

$$D = \frac{0.9 \times \lambda}{\beta \times \cos\theta} \qquad \text{(Eq.2)}$$

Where D is the crystalline size (nm), λ the wavelength of the X-ray radiation (0.154056 nm), θ the Bragg's angle and β is the peak width at half maximum (FWHM) for major diffraction peak.
Fourier transform infrared spectra were obtained by using a VERTEX 70 spectrophotometer. Measurements were performed in the transmission mode in spectroscopic grade KBr pellets. BET specific surface area was determined by the multipoint method using the adsorption data of $N_2$ at 77K. Samples microstructure and composition were analyzed by recording transmission electron microscopy using a FEI TECNAI G2 instrument operated at an accelerating voltage of 120 KV.

*2.3 Photocatalytic experiments*
Photocatalytic experiments were performed in cylindrical batch reactor with 10 cm in diameter and 20 cm in height as depicted in our previous works [31]. The reactor was made from quartz glass, which made possible the transfer of the irradiation. The reactor was exposed to a luminous source composed of a medium pressure mercury-lamp (400 W), placed in axial position inside a cooling water jacket system. Constant agitation was assured by means of a magnetic stirrer placed at reactor base.
The reactor was initially loaded with 800 ml of 2,4-D or 2,4-DP aqueous solutions at an initial concentration of 20 mg/L. The mass of the photocatalyst was 120 mg. The mixture was maintained in the dark for 30 min under stirring to reach adsorption equilibrium, and was then irradiated. Samples taken at different irradiation times were centrifuged at 3000 tr/min for 10 min. The residual concentration was determined from its UV absorbance characteristic with the calibration curve method at the wavelength of maximum absorption ($\lambda_{max}$) of 283 nm for 2,4-D and 284 nm for 2,4-DP. A GBC UV/Vis 911 spectrophotometer was used.

## 3. Results and discussion

*3.1. XRD characterization of the photocatalysts*
Figure.1 shows the XRD patterns of synthesized $TiO_2$ and x%-W/$TiO_2$ photocatalysts. Most of the peaks in XRD pattern of $TiO_2$ (Figure.1a) are attributed to those of anatase phase. A broad and weak peak at 31.6° was attributed to the rutile phase. The diffraction angles (2θ) of 25.3° 37.79°, 48°, 53.88°, 55°, 63.8°, 72°, 75° and 31.6° represent respectively the (101), (004), (200), (105), (211), (104), (216), (215) crystal face of anatase and the (103) crystal face of rutile. The fineness peaks indicates that the nanosized materials were well crystallized. The ratio of rutile was 11.5% while that of the anatase phase was 88.5 %.
The XRD patterns of different x%-W/$TiO_2$ samples showed only the peaks of anatase phase. The absence of the sole characteristic peak of the rutile phase can be explained by the stabilization of the anatase phase from transformation into inactive rutile phase. The peaks observed especially in the sample 4%-W/$TiO_2$ at 2θ of 27.5, 36.2 and 38.6° are attributed to the $WO_3$ crystalline phase. No characteristic bands due to crystalline $WO_3$ were observed in the samples 1%-W/$TiO_2$ and 2,5%-W/$TiO_2$ which indicates clearly that the tungsten oxide is highly dispersed on this photocatalysts. Others studies have reported that no $WO_3$ phase observed up to 20 wt% [29, 33].
The estimated average particle sizes were 2.3561 nm, 3.0331 nm, 3.0377 nm and 3.5527 nm for $TiO_2$, 1%-W/$TiO_2$, 2.5%-W/$TiO_2$ and 4%-W/$TiO_2$, respectively. The crystalline size of tungsten loaded titanium dioxide samples increases by increasing the impregnated amounts of $WO_3$.

*3.2. FT-IR spectra of $TiO_2$ and tungsten loaded $TiO_2$*
Figure 2 shows FT-IR spectra of synthesized $TiO_2$ and tungsten loaded titanium dioxide samples. The anatase phase of titania exhibits strong absorption bands at 640, 1632 and 3401 $cm^{-1}$. No rutile phase peak is detected in this experiment, because of the limit of the employed instrument. The presence of these bands due to $TiO_2$ anatase phase is noted for both samples. Generally, bands situated at 3401 $cm^{-1}$ and at 1632 $cm^{-1}$, are attributed respectively to the stretching and bending, of the Ti-OH groups [29,34]. The bands situated in the region 800-400 $cm^{-1}$ are assigned to the deformation mode of Ti-OH and Ti-O-Ti groups [35-37]. No characteristic bands due to the crystalline $WO_3$ were observed this indicates clearly that the tungsten oxide is highly dispersed on the $TiO_2$.

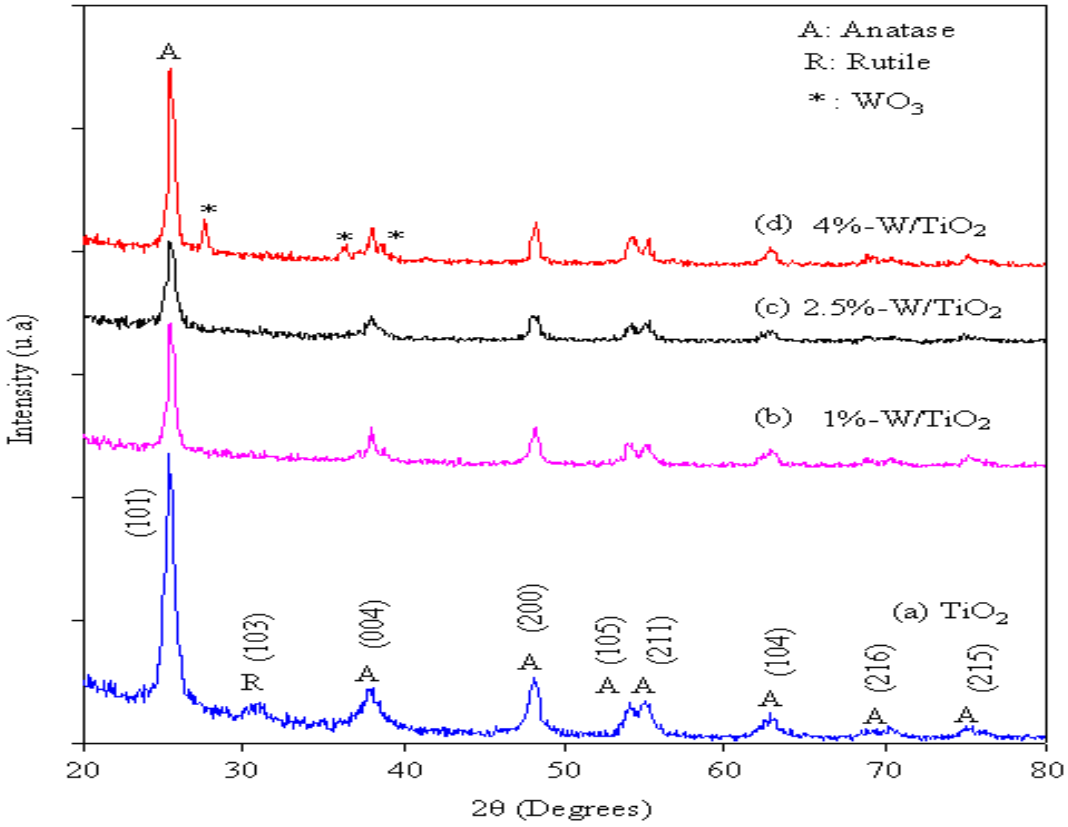


**Figure 1:** XRD patterns of synthesized $TiO_2$ (a), 1%-W/$TiO_2$ (b), 2.5%-W/$TiO_2$ (c) and 4%-W/$TiO_2$ (d).

*3.3. Surface area analyses*

Specific surface areas of $TiO_2$ and x%-W/$TiO_2$ samples are given in Table 1. The calculated specific surface area of $TiO_2$ was 67.66 $m^2/g$. After impregnation with $WO_3$ a small decrease in the specific surface area can be noted. As the amounts of tungsten loaded on $TiO_2$ increased, the specific surface area of the samples has decreased. This is primarily due to a high dispersion of tungsten oxide in the surface pores of $TiO_2$.

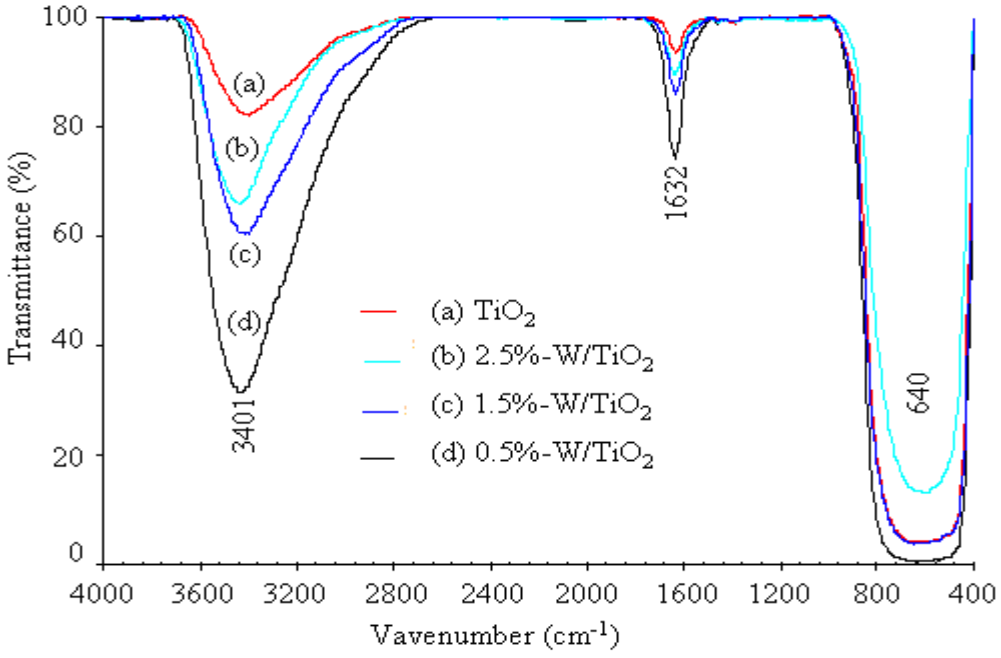


**Figure 2:** FT-IR spectra of $TiO_2$ (a), 2.5%-W/$TiO_2$ (b), 1.5%-W/$TiO_2$ (c) and 0.5%-W/$TiO_2$ (d).

**Table 1:** Specific surface areas of the photocatalysts investigated in this study.

| Catalysts samples | BET surface area ($m^2/g$) |
|---|---|
| $TiO_2$ | 67.66 |
| 1%-W/$TiO_2$ | 66.16 |
| 2.5%-W/$TiO_2$ | 61.18 |
| 4%-W/$TiO_2$ | 58.84 |

*3.4. TEM-EDX analyses*

TEM and EDX were used to study, respectively, the morphologies and elemental distribution of the samples. Figure 3 presents the TEM morphologies and EDX patterns of the synthesized $TiO_2$ and 1.5%-W/$TiO_2$. Apparently, TEM micrographs and EDX patterns for the surfaces samples exhibited similar morphologies and elemental distributions. It clearly showed that both these samples were nanosized particles. The particles possess a uniform distribution. The tungsten possesses a covalent radius of 1,30 Å and ray to states $W^{4+}$ and $W^{6+}$ respectively of the order of 0.70 Å and 0.62 Å. The titanium in the state $Ti^{4+}$ possesses an ionic radius of the order of 0.68 Å. Consequently, the ion $W^{6+}$ and/or $W^{4+}$ can be easily inserted inside the of $TiO_2$ structure. In particular, the insertion of the ions $W^{6+}$ is made without distortion of the structure $TiO_2$. The energy dispersive X-ray spectra of 1.5%-W/$TiO_2$ reveal the presence of C, O, Ti, Cu and in particular the tungsten. The peaks of energy at 1.8 and 8.8 KeV are attributed to tungsten W (Figure 3d).

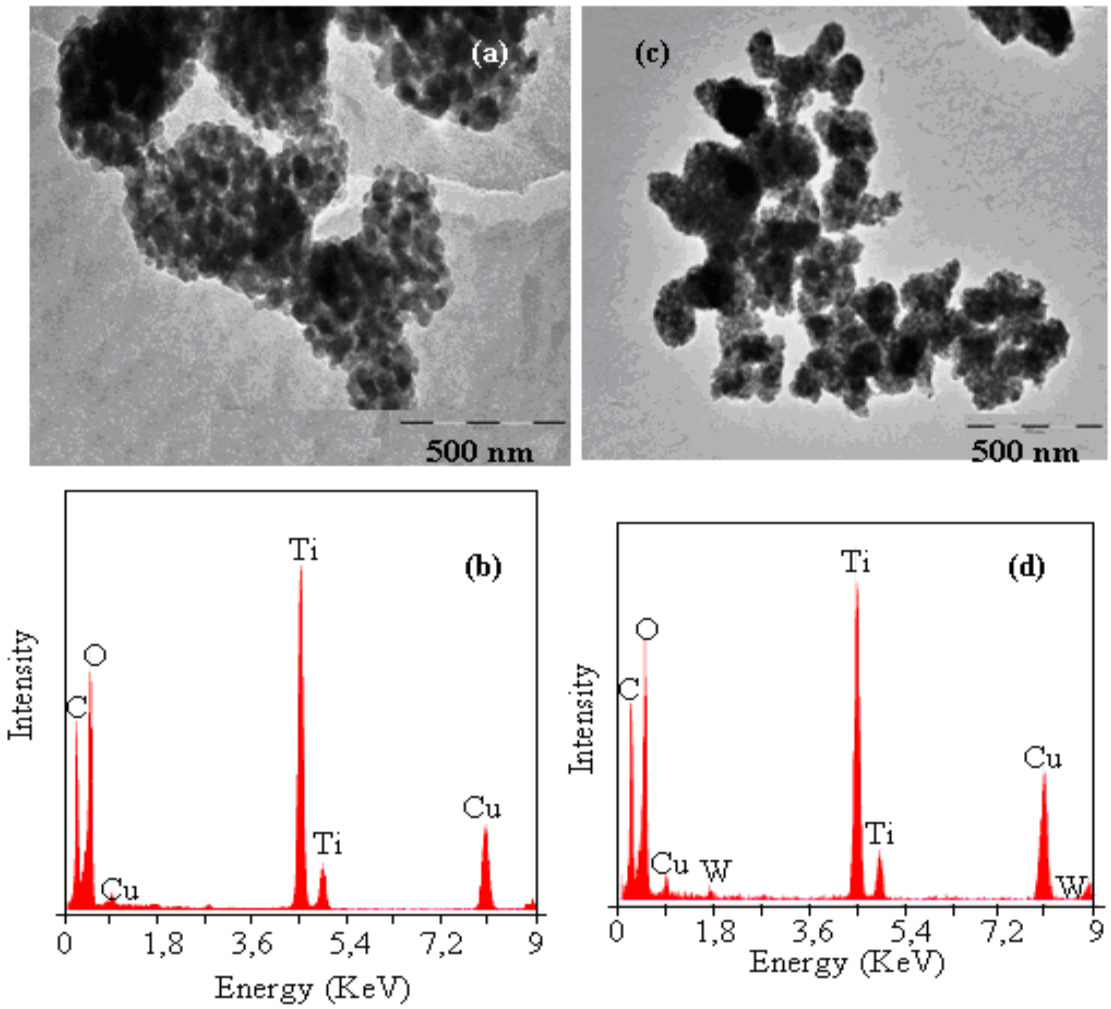


**Figure 3:** TEM micrographs and EDX patterns of $TiO_2$ (a) and (b), 1,5%-W/$TiO_2$ tungsten (c) and (d).

*3.5. Photocatalytic performance*

*3.5.1. Persistence of 2,4-D under UV irradiation*

In the same operating conditions used for the photocatalytic degradation, the photolytic degradation was studied using 800 ml of 2,4-D and 2,4 DP at an initial concentration of 20 mg/L. The solution was irradiated without photocatalysts. The results are illustrated in Figures 4 and 5. Kinetics of pesticides photolytic degradation shows that, after 90 min of irradiation, a very low diminution of the concentration was observed. From this result, we can neglect the interference of the photolytic degradation with the photocatalytic degradation.

*3.5.2. Preliminary adsorption in the dark*

Sorption is an important parameter in determining photocatalytic degradation rate. The adsorbed molecules on the surface of the semiconductor particles act as an electron donor, injecting electrons from its excited state to the conduction band of the semiconductor under UV irradiation [38, 39]. Adsorption tests in the dark were carried out in order to evaluate the adsorbed quantities of 2,4-D and 2,4-DP on the photocatalysts. Table 2 shows that the adsorbed quantities of the two pesticides do not exceed 7 % of the initial quantity in the solution. The adsorbed quantities of 2,4-D and 2,4-DP on tungsten loaded $TiO_2$ increases with the augmentation of tungsten content. This result can be explained by availability of more adsorption sites at the surface of the photocatalysts.

**Table 2: A**dsorbed quantities (mg/g) of used pesticides on the photocatalysts.

| Photocatalysts | 2,4-D | 2,4-DP |
|---|---|---|
| $TiO_2$ | 6.35 | 6.41 |
| 0.5%-W/$TiO_2$ | 6.29 | 6.29 |
| 1%-W/$TiO_2$ | 6.35 | 7.14 |
| 2.5%-W/$TiO_2$ | 7.42 | 7.41 |
| 4%-W/$TiO_2$ | 7.54 | 8.41 |

*3.5.3. Photocatalytic degradation*

The photocatalytic performance of the $TiO_2$ and tungsten loaded $TiO_2$ samples for the degradation of 2,4-D and 2,4-DP is shown in figures 4,5.

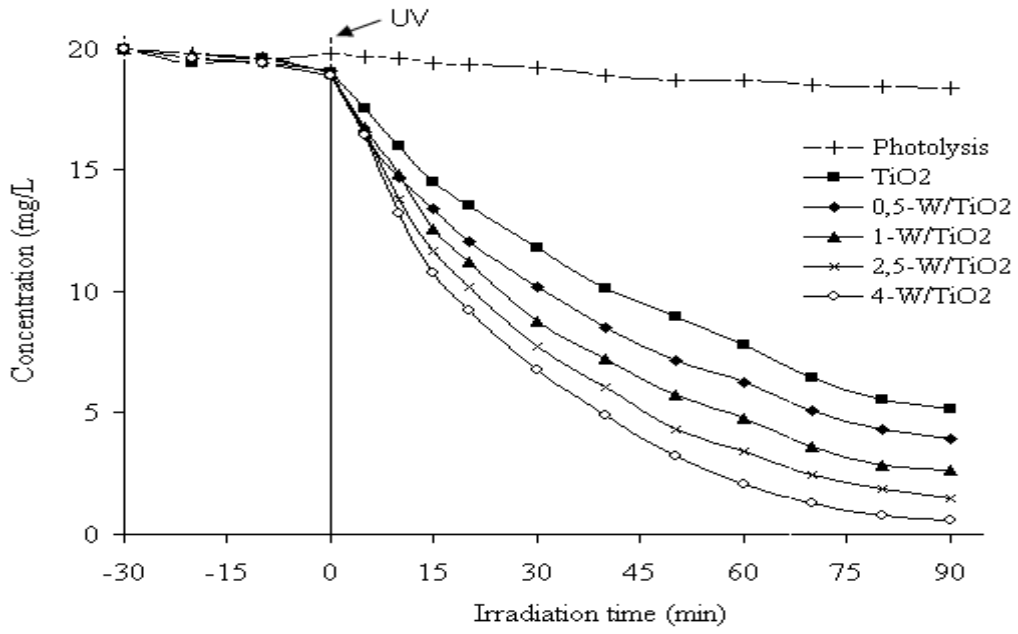


**Figure 4:** Variation of 2,4-D concentration versus irradiation time without and with the photocatalysts.

The figures indicate that the photocatalytic activities of tungsten doped titanium oxide samples were higher than that of $TiO_2$ catalyst. This result could be due to the fact that the structure defects on the surface of metal oxides enhances the $O^-$ species sorbed, which can cause hole trap reaction and produces more $OH^\bullet$ radical that are involved in the degradation of organic compounds by photocatalysis. The degradation rate was found to increase consequentially with the increase of W loading. The order of catalytic activity for 2,4-D and 2,4-DP was 4%-W/$TiO_2$ > 2.5%-W/$TiO_2$ > 1%-W/$TiO_2$ > 0.5%-W/$TiO_2$ > $TiO_2$.
A possible explanation of the catalytic activity order can be mainly attributed to the bad gap energy reduction, long-term life of electron/hole during semiconductor illumination under UV light. The band gap of $WO_3$ is 2.5 eV, which corresponds to absorption out to approximately 500 nm, well into the visible. Moreover, because of the absolute positions of the bands, electrons from conduction bond of $TiO_2$ can migrate to $WO_3$, while the complementary migration can occur for valence band holes. Similar observation has also been reported by Hathway et al. [30]. However, this observation shows that the highest catalytic activity is due in large part to the extended near-visible absorption of the anatase phase, followed by rapid electron transfer between the phases, leading to enhanced charge separation and reduced energy wastage by electron-hole recombination.

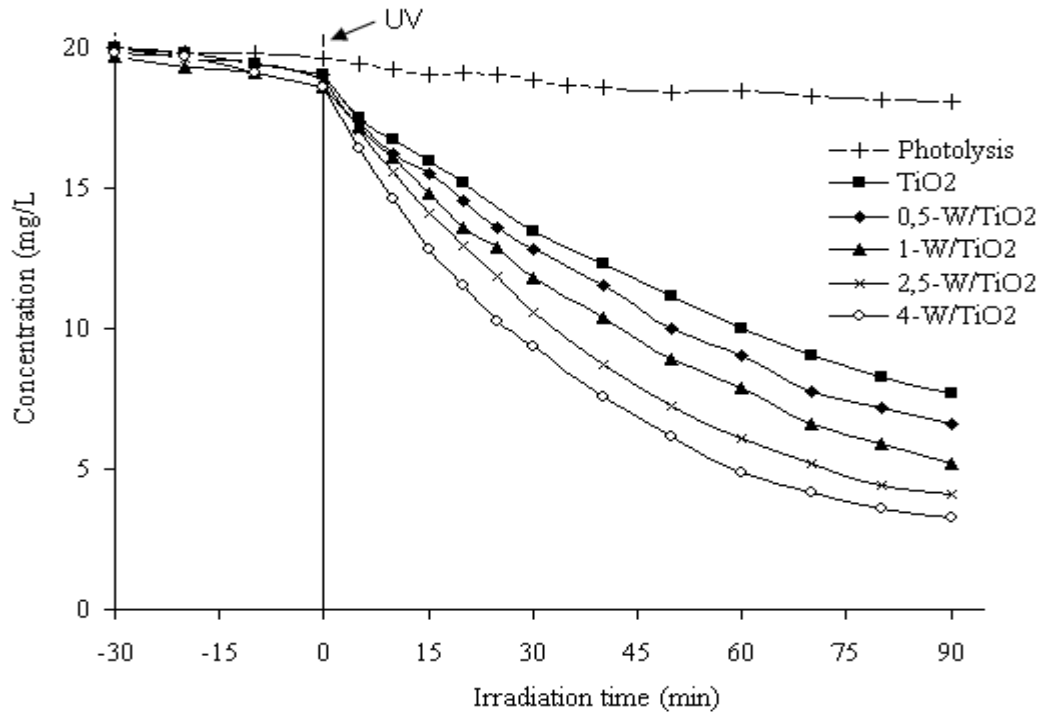


**Figure 5:** Variation of 2,4-DP concentration versus irradiation time without and with the photocatalysts**.**

## 4. Conclusions

Titanium dioxide and tungsten doped titanium dioxide were successfully synthesized by the sol-gel method. X-ray powder diffraction, FT-IR spectroscopy, BET surface area and transmission electron microscopy coupled to energy dispersive spectroscopy confirmed the formation of good quality crystalline nanomaterials. A perfect match was found between the tungsten amounts loading in the catalyst and the photocatalytic degradation efficiency. The x%-W/$TiO_2$ catalysts calcined at 500°C also retain the $TiO_2$-anatase phase of the support and the impregnated tungsten oxide being in a highly dispersed state. The apparently increase in tungsten loading stabilized the anatase phase from transformation into inactive rutile, accompanied by increase of doped grain size and a few decrease in BET surface area. All the doped samples exhibit better catalytic performance than the unmodified $TiO_2$ sample. The photocatalytic activity also depends on the type of the model pollutant.

## References

1. Ollis, D.F., Pelezzetti, E., Serpone, N., *Environ. Sci. Technol.* 25 (1991) 1522.
2. Fassi, S., Bousnoubra, I., Sehili, T., Djebbar, K., *J. Mater. Environ. Sci*. 3 (4) (2012) 732.
3. Barka, N., Qourzal, S., Assabbane, A., Nounah, A., Ait-Ichou, Y., *Chem. Eng. comm.* 198 (2011) 1233.

4. Alahiane, S., Qourzal, S., El Ouardi, M., Belmouden, M., Assabbane, A., Ait-Ichou, Y., *J. Mater. Environ. Sci. 4 (2)* (2013) 239.
5. Barka, N., Qourzal, S., Assabbane, A., Nounah, A., Ait-Ichou, Y., *Arab. J. Chem.* 3 (2010) 279.
6. Qourzal, S., Barka, N., Belmouden, M., Abaamrane, A., Alahiane, S., Elouardi, M., Assabbane, A., Ait-Ichou, Y., *Fresenius Environ. Bulletin* 21(7) (2012) 1972.
7. Abdennouri, M., Galadi, A., Barka, N., Baâlala, M., Nohair, K., Elkrati, M., Sadiq, M., Bensitel, M., Phys. *Chem. News* 54 (2010) 126.
8. Vulliet, E., Chovelon, J.M., Guillard, C., Herrmann, J.M., *J. Photochem. Photobiol. A: Chem.* 159 (2003) 71.
9. Xia, B., Huang, H., Xie, Y., *Mater. Sc.Eng.* B57 (1999) 150.
10. Qourzal, S., Barka, N., Tamimi, M., Assabbane, A., Nounah, A., Ihlal, A., Aît Ichou, Y., *Mater. Sc. Eng. C* 29 (2009) 1616.
11. Bayati, M.R., Golestani-Fard, F., Moshfegh, A.Z., *Appl. Catal. A: Gen.* 382 (2010) 322.
12. Abdennouri, M., Baâlala, M., Galadi, A., El Makhfouk, M., Bensitel, M., Nohair, K., Sadiq, M., Barka N., *Arab. J. Chem.* (2011), doi:10.1016/j.arabjc.2011.04.005.
13. Riyas, S., Yasir, V.A., Mohan Das, P.N., *Bull. Mater. Sci.* 25 (2002) 267.
14. Sankar, G., Kannan, K., Rao, C., *Catal. Lett.* 8 (1991) 27.
15. Reddy, B.M., Reddy, E.P., Mehdi, S., *Mater. Chem. Phys.* 36 (1994) 276.
16. Barakat, M., Hayes, G., Shah, S., *J. Nanosci. Nanotechnol*. 5 (2005) 759.
17. Mahanty, S., Roy, S., Sen, S., *J. Cryst. Growth* 261 (2004) 77.
18. Sen, S., Mahanty, S., Roy, S., Heintz, O., Bourgeois, S., Chaumont, D., *Thin Solid Films* 474 (2005) 245.
19. Venkatachalam, N., Palanichamy, M., Arabindoo, B., Murugesan, V., *Catal. Commun.* 8 (2007) 1088.
20. Arroyo, R., Cordoba, G., Padilla, J., Lara, V., *Mater. Lett.* 54 (2002) 397.
21. Saif, M., Abdel-Mottaleb, M.S.A., *Inorg. Chim. Acta* 360 (2007) 2863.
22. Parida, K.M., Sahu, N., *J. Mol. Catal. A: Chem.* 287 (2008) 149.
23. Ahmad, A., Buzby, S., Ni, C., Shah, S.I., *J. Nanosci. Nanotechnol.* 8 (2008) 2410.
26. Di Paola, A., Garcia-Lóopez, E., Marci, G., Martin, C., Palmisano, L., Rives, V., Venezia, A.M., *Appl. Catal. B: Environ.* 48 (2004) 223.
27. Gong, J.Y., Yang, C.Z., Pu, W.H., Zhang, J.D., *Chem. Eng. J.* 167 (2011) 190.
28. Leghari, S.AK., Sajjad, S., Chen, F., Zhang, J., *Chem. Eng. J.* 166 (2011) 906.
29. Saepurahman, Abdullah, M.A., Chong, F.K., *J. Hazard. Mater.* 176 (2010) 451.
30. Hathway T., Rockafellow E.M., Oh, Y.C., Jenks, W.S., *J. Photochem. Photobiol. A : Chem.* 207 (2009) 197.
31. Barka, N., Abdennouri, M., Boussaoud, A., Galadi, A., Baâlala, M., Bensitel, M., Sahibed-Dine, A., Nohair, K., Sadiq, M., *Arab. J. Chem. (2011), doi:10.1016/j.arabjc.2010.12.015*
32. Jongsomjit, B., Wongsalee, T., Praserthdam, P., *Mater. Chem. Phys.* 92 (2005) 572.
33. Arroyo, R., Cordoba, G., Padilla, J., Lara, V., *Mater. Lett.* 54 (2002) 397.
34. Bezrodna, T., Puchkovska, G., Shymanovska, V., Baran, J., Ratajczak, H., *J. Mol. Struct.* 700 (2004) 175.
35. Chen, Y-F., Lee, C-Y., Yeng, M-Y., Chiu, H-T., *J. Cryst. Growth* 247 (2003) 363.
36. Ivanda, M., Musić, S., Popović, S., Gotić, M., *J. Mol. Struct.* 480-481 (1999) 645.
37. Khalil, K.M.S., Baird, T., Zaki, M.I., El-Samahy, A.A., Awad, A.M., *Colloids Surf. A* 132 (1998) 31.
38. Barka, N., Assabbane, A., Nounah, A., Aît Ichou, Y., *J. Hazard. Mater.* 152 (2008) 1054–1059.
39. Barka, N., Qourzal, S Assabbane, A., Nounah, A., Aît Ichou, Y., *J. Photochem. Photobiol. A: Chem.* 195 (2008) 346.